

Focusing coherent light through opaque strongly scattering media

I. M. Vellekoop* and A. P. Mosk

Complex Photonic Systems, Faculty of Science and Technology and MESA+ Research Institute,
University of Twente, P.O. Box 217, 7500 AE Enschede, The Netherlands

*Corresponding author: i.m.vellekoop@utwente.nl

Received March 6, 2007; revised June 14, 2007; accepted June 21, 2007;
posted June 28, 2007 (Doc. ID 80762); published August 2, 2007

We report focusing of coherent light through opaque scattering materials by control of the incident wavefront. The multiply scattered light forms a focus with a brightness that is up to a factor of 1000 higher than the brightness of the normal diffuse transmission. © 2007 Optical Society of America

OCIS codes: 290.1990, 290.4210, 030.6600.

Random scattering of light is what makes materials such as white paint, milk, or human tissue opaque. In these materials, repeated scattering and interference distort the incident wavefront so strongly that all spatial coherence is lost [1]. Incident coherent light diffuses through the medium and forms a volume speckle field that has no correlations on a distance larger than the wavelength of light. The complete scrambling of the field makes it impossible to control light propagation using the well-established wavefront correction methods of adaptive optics (see e.g., [2]).

We demonstrate focusing of coherent light through disordered scattering media by the construction of wavefronts that invert diffusion of light. Our method relies on interference and is universally applicable to scattering objects regardless of their constitution and scattering strength. We envision that, with such active control, random scattering will become beneficial, rather than detrimental, to imaging [1] and communication [3–5].

Figure 1 shows the principle of the experiment. Normally, incident light is scattered by the sample and forms a random speckle pattern [Fig. 1(a)]. The goal is to match the incident wavefront to the sample so that the scattered light is focused in a specified target area [Fig. 1(b)]. The experimental setup for constructing such wavefronts is shown in Fig. 2. Light from a 632.8 nm HeNe laser is spatially modulated by a liquid-crystal phase modulator and focused on an opaque, strongly scattering sample. The number of degrees of freedom of the modulator is reduced by grouping pixels into a variable number (N) of square segments. A CCD camera monitors the intensity in the target focus and provides feedback for an algorithm that programs the phase modulator.

We performed first tests of inverse wave diffusion using rutile (TiO_2) pigment, which is one of the most strongly scattering materials known. The sample consists of an opaque, 10.1- μm -thick layer of rutile [6] with a transport mean free path of $0.55 \pm 0.10 \mu\text{m}$ measured at $\lambda = 632.8 \text{ nm}$. Since in this sample the transmitted light is scattered hundreds of times, there is no direct relation between the incident wavefront and the transmitted image [7,8].

In Fig. 3 we show the intensity pattern of the transmitted light. In Fig. 3(a) we see the pattern that was transmitted when a plane wave was focused onto the sample. The light formed a typical random speckle pattern with a low intensity. We then optimized the wavefront so that the transmitted light focused to a target area with the size of a single speckle. The result for a wavefront composed of 3228 individually controlled segments is seen in Fig. 3(b), where a single bright spot stands out clearly against the diffuse background. The focus was over a factor of 1000 more intense than the nonoptimized speckle pattern. By adjusting the target function used as feedback it is also possible to optimize multiple foci simultaneously, as is shown in Fig. 3(c) where a pattern of five spots was optimized. Each of the spots has an intensity of approximately 200 times the original diffuse intensity. In Fig. 3(d) we show the phase of the incident wavefront corresponding to Fig. 3(c). Neighboring segments are uncorrelated, which indicates that the sample fully scrambles the incident wavefront.

The algorithm that constructs the inverse diffusion wavefront uses the linearity of the scattering process. The transmitted field in the target, E_m , is a linear combination of the fields coming from the N different segments of the modulator:

$$E_m = \sum_{n=1}^N t_{mn} A_n e^{i\phi_n}, \quad (1)$$

where A_n and ϕ_n are, respectively, the amplitude and phase of the light reflected from segment n . Scatter-

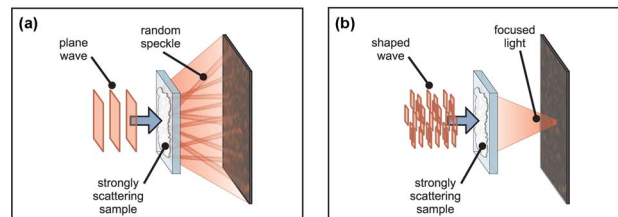


Fig. 1. (Color online) Design of the experiment. (a) A plane wave is focused on a disordered medium, and a speckle pattern is transmitted. (b) The wavefront of the incident light is shaped so that scattering makes the light focus at a predefined target.

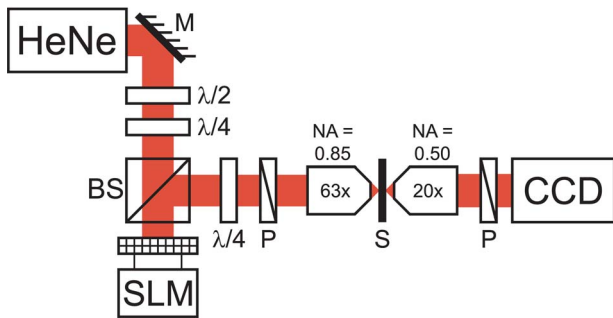


Fig. 2. (Color online) Schematic of the apparatus. A 632.8 nm HeNe laser beam is expanded and reflected off a Holoeye LR-2500 liquid crystal spatial light modulator (SLM). Polarization optics select a phase mostly modulation mode. The SLM is imaged onto the entrance pupil of the objective with a 1:3 demagnifying lens system (not shown). The objective is overfilled; we use only segments that fall inside the pupil. The shaped wavefront is focused on the strongly scattering sample (S), and a CCD camera images the transmitted intensity pattern. $\lambda/4$, quarter-wave plate; $\lambda/2$, half-wave plate; M, mirror; BS, 50% non-polarizing beam splitter; P, polarizer.

ing in the sample and propagation through the optical system is described by the elements t_{mn} of the unknown transmission matrix. Clearly, the magnitude of E_m will be the highest when all terms in Eq. (1) are in phase. We determine the optimal phase for a single segment at a time by cycling its phase from 0 to 2π . For each segment we store the phase at which the target intensity is the highest. At that point the contribution of the segment is in phase with the already present diffuse background. After the measurements have been performed for all segments, the phase of the segments is set to their stored values. Now the contributions from all segments interfere constructively and the target intensity is at the global maximum. A preoptimization with a small number of segments significantly improves the signal-to-noise ratio. This method is generally applicable to linear systems and does not rely on time reversal symmetry or absence of absorption. Although mathematically this algorithm is the most efficient, in noisy experimental conditions adaptive learning algorithms [9] might be more effective, and an investigation of such algorithms is on its way.

The maximum intensity enhancement that can be reached is related to the number of segments that are used to describe the incident wavefront. For a disordered medium the constants t_{mn} are statistically independent and obey a circular Gaussian distribution [8,10–12], and the expected enhancement η , defined as the ratio between the optimized intensity and the average intensity before optimization, can be calculated:

$$\eta = \frac{\pi}{4}(N - 1) + 1. \quad (2)$$

It was assumed that all segments of the phase modulator contribute equally to the total incident intensity. We expect the linear scaling behavior to be universal as Eq. (2) contains no parameters. Also, since

we are free to choose the basis for Eq. (1), we expect to find the same enhancement regardless of whether the target is a focus or a far-field beam and regardless of how the shaped wavefront is projected onto the sample. Interesting correlations between the transmission matrix elements, which will cause corrections on Eq. (2), are predicted when N approaches the total number of mesoscopic channels [11,12]. With our current apparatus we are far from this regime and no deviation from Eq. (2) is expected.

We tested the universal scaling behavior implied by Eq. (2) by changing N . Using the same TiO_2 sample as before, the algorithm was targeted to construct a collimated beam. In Fig. 4 the enhancement is plotted as a function of the number of segments for different focusing conditions. The linear relation between the enhancement and the number of segments is evident until the enhancement saturates at $\eta = 1000$. All measured enhancements were slightly below the theoretical maximum. This is understandable since all perturbations move the system away from the global maximum. The main reason for deviations from the optimal wavefront is residual amplitude modulation in the phase modulator, which introduced an uncontrolled bias in the field amounting to 14% of the total intensity.

The saturation of the enhancement is the result of slow changes in the speckle pattern. This instability effectively limited the number of segments for which the optimal phase could be measured. We estimate that the effective enhancement decreases to $\eta_{\text{eff}} = \eta/(1 + NT/T_p)$, where $T = 1.2$ s is the time needed for one measurement and the persistence time $T_p = 5400$ s is the time scale at which the speckle pattern of the TiO_2 sample remains stable. Depending on the environmental conditions, T_p can be consider-

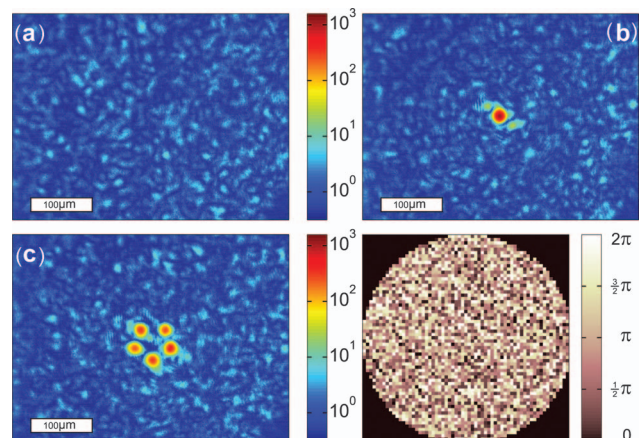


Fig. 3. Transmission through a strongly scattering sample consisting of TiO_2 pigment. (a) Transmission micrograph with an unshaped incident beam. (b) Transmission after optimization for focusing at a single target. The scattered light is focused to a spot that is 1000 times brighter than the original speckle pattern. (c) Multibeam optimization. The disordered medium generates five sharp foci at the defined positions. (a)–(c) are presented on the same logarithmic color scale that is normalized to the average transmission before optimization. (d) Phase of the incident wavefront used to form (c).

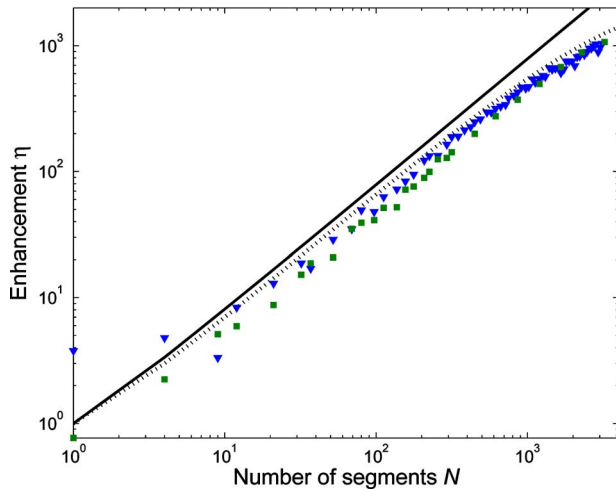


Fig. 4. (Color online) Measured intensity enhancement as a function of the number of segments. Squares, sample in focus; triangles, sample 100 μm behind focus; solid curve, ideal enhancement [Eq. (2)], dotted curve, corrected for residual amplitude modulation and finite persistence time of $T_p = 5400$ s. The experimental uncertainty is of the order of the symbol size.

Table 1. Measured Intensity Enhancement for Different Materials^a

Sample	L (μm)	η ($\pm 15\%$)	N
Rutile TiO_2	10.1 ± 0.3	1080	3228
Daisy petal, fresh	43 ± 5	64	208
Daisy petal, dried	37 ± 5	630	1664
Chicken eggshell	430 ± 30	250	3228
Human tooth	1500 ± 100	70	208

^a L , sample thickness (\pm surface roughness); η , maximum enhancement reached; N , number of segments used by the algorithm to describe the wavefront.

ably higher and enhancements of over 2000 have been measured overnight.

To verify the universal applicability of inversion of wave diffusion, we used a variety of materials of natural origin. Table 1 lists the intensity enhancement for different materials we used. Although the samples vary in thickness, composition, and scattering strength, they were all able to focus a properly prepared wavefront to a sharp spot. The intensity enhancement varies between 60 and 1000. The main reason for this variation is that the persistence time is not the same for all materials.

In summary, our results show that precise control of diffuse light is possible using an optimal, noniterative algorithm; light can be directed through opaque objects to form one or multiple foci. The brightness of

the focal spot is explained by a model based on statistical optics. We expect inverse wave diffusion to have applications in imaging and light delivery in scattering media, possibly including metal nanostructures [13]. Dynamic measurements in biological tissue are possible when the time required for achieving a focus can be reduced to below 1 ms per segment [14,15]; we estimate that this time scale is technologically possible with the use of fast phase modulators [16]. Furthermore, the high degree of control over the scattered light should permit experimental verification of random matrix theories for the transport of light [11,12].

We thank Ad Lagendijk for valuable discussions, Willem Vos and Vinod Subramaniam for a critical reading of the manuscript, and the Photon Scattering group of the Institute for Atomic and Molecular Physics (AMOLF) for providing samples. This work is part of the research program of the Stichting voor Fundamenteel Onderzoek der Materie (FOM), which is financially supported by the Nederlandse Organisatie voor Wetenschappelijk Onderzoek (NWO).

References

1. P. Sebbah, ed., *Waves and Imaging through Complex Media* (Kluwer, 2001).
2. R. K. Tyson, *Principles of Adaptive Optics* (Academic, 1998).
3. A. Derode, A. Tourin, J. de Rosny, M. Tanter, S. Yon, and M. Fink, *Phys. Rev. Lett.* **90**, 014301 (2003).
4. S. H. Simon, A. L. Moustakas, M. Stoytchev, and H. Safar, *Phys. Today* **54**(9), 38 (2001).
5. G. Leroosey, J. de Rosny, A. Tourin, and M. Fink, *Science* **315**, 1120 (2007).
6. R. H. J. Kop, P. de Vries, R. Sprik, and A. Lagendijk, *Phys. Rev. Lett.* **79**, 4369 (1997).
7. R. Pappu, B. Recht, J. Taylor, and N. Gershenfeld, *Science* **297**, 2026 (2002).
8. J. W. Goodman, *Statistical Optics* (Wiley, 2000).
9. D. E. Goldberg, *Genetic Algorithms in Search, Optimization and Machine Learning* (Addison-Wesley, 1989).
10. N. Garcia and A. Z. Genack, *Phys. Rev. Lett.* **63**, 1678 (1989).
11. C. W. J. Beenakker, *Rev. Mod. Phys.* **69**, 731 (1997).
12. J. B. Pendry, A. MacKinnon, and P. J. Roberts, *Proc. R. Soc. London, Ser. A* **437**, 67 (1990).
13. M. I. Stockman, S. V. Faleev, and D. J. Bergman, *Phys. Rev. Lett.* **88**, 067402 (2002).
14. B. J. Vakoc, S. H. Yun, J. F. de Boer, G. J. Tearney, and B. E. Bouma, *Opt. Express* **13**, 5483 (2005).
15. J. Li, G. Dietsche, D. Iftime, S. E. Skipetrov, G. Maret, T. Elbert, B. Rockstroh, and T. Gislser, *J. Biomed. Opt.* **10**, 044002 (2005).
16. M. Hacker, G. Stobrawa, R. Sauerbrey, T. Buckup, M. Motzkus, M. Wildenhain, and A. Gehner, *Appl. Phys. B: Lasers Opt.* **76**, 711 (2003).